Journal of the American Chemical Society **2021**, *143*, 16332−16336 - DOI: 10.1021/jacs.1c07186

Real-time observation of 'soft' magic size clusters during hydrolysis of the model metallodrug bismuth di-salicylate

Daniel Szczerba‡[1], Davin Tan‡[2], Jean-Louis Do[2], Hatem M. Titi[2], Siham Mouhtadi[3], Denis Chaumont[1], María del Carmen Marco de Lucas[1], Nicolas Geoffroy[1], Michel Meyer[4], Yoann Rousselin[4], Jessica M. Hudspeth[5], Valérie Schwanen[6], Petra Spoerk-Erdely[7], Ann-Christin Dippel[8], Oleh Ivashko[8], Olof Gutowski[8], Philipp Glaevecke[8], Vasilli Bazhenov[9], Mihails Arhangelskis[10], Ivan Halasz[11], Tomislav Friščić*[2], and Simon A.J. Kimber*[1]

[1] Laboratoire Interdisciplinaire Carnot de Bourgogne, UMR 6303, CNRS, Université Bourgogne Franche-Comté, 9 avenue Alain Savary, BP 47870, 21078 Dijon Cedex, France

[2] Department of Chemistry, McGill University, Montréal, QC H3A 0B8, Canada

[3] Université Franche-Comté, Insitut UTINAM-Équipe MSF, and Université Bourgogne Franche-Comté, 25030 Besançon, France

[4] Insitut de Chimie Moléculaire de l'Université de Bourgogne, UMR 6302, CNRS, Université Bourgogne Franche-Comté, 9 Avenue Alain Savary, BP 47870, 21078 Dijon Cedex, France

[5] European Synchrotron Radiation Facility, BP 156, 38042, Grenoble, France

[6] University of Liège, Allée du six août, 11 - 4000 Liège, Belgium

[7] Department Materials Science, Montanuniversität Leoben, Franz Josef-Strasse 18, 8700 Leoben, Austria.

[8] Deutsches Elektronen-Synchrotron DESY, Notkestraße. 95, 22603 Hamburg, Germany

[9] European XFEL GmbH, Holzkoppel 4, 22869 Schenefeld, Germany

[10] Faculty of Chemistry, University of Warsaw, 1 Pasteura St. 02-093 Warsaw, Poland

[11] Ruđer Bošković Institute, Bijenička cesta 54, 10000 Zagreb, Croatia

‡*These authors contributed equally,* **tomislav.friscic@mcgill.ca,* **simon.kimber@u-bourgogne.fr*

ABSTRACT: Colloidal bismuth therapeutics have been used for hundreds of years, yet remain mysterious. Here we report an X-ray pair distribution function (PDF) study of the solvolysis of bismuth di-salicylate, a model for the metallodrug bismuth subsalicylate (Pepto-Bismol©). This reveals catalysis by traces of water, followed by multi-step cluster growth. The ratio of the two major species, $\{Bi_9O_7\}$ and $\{Bi_{38}O_{44}\}$, depends on exposure to air, time, and the solvent. The solution-phase cluster structures are of significantly higher symmetry than solid-state analogues, with reduced off-centre Bi^{3+} displacements. This explains why such 'magic size' clusters can be both stable enough to crystallise, yet sufficiently labile for further growth.

Metallodrugs have been used therapeutically since antiquity[1,2]. Those based upon bismuth suboxides are known for antibacterial and antiviral properties[3,4], with bismuth subsalicylate (Pepto-Bismol©) used to treat infection by *Helicobacter pylori* and ranitidine bismuth citrate shown to inhibit COVID-19 replication[5]. Despite this history, the structures of many Bi metallodrugs are unknown[3], due to the rich hydrolysis chemistry of bismuth, which forms poorly characterised colloids, with multiple cluster sizes[6–12].

Such unconventional nucleation and growth mechanisms imply metastable species trapped in local energetic minima[13,14]. When intermediates can be crystallised, they are often found to be 'magic size' clusters, i.e. containing closed geometric shells of atoms or valence electrons[15,16]. However, the relevance of such 'frozen' solid-state structures to solution-phase reactivity is unclear. In fact, magic size gold nanoparticles have been shown to exist in multiple polymorphs[17], and CdS clusters undergo isomerisation driven by surface coordination[18]. Such 'softness' might explain why clusters can be simultaneously stable enough to crystallise, but also sufficiently labile to participate in further growth. This question is important for metallodrugs, and has much wider implications for e.g. bio-mineralisation[19], geological settings[20] and nuclear chemistry[21].

Here, we use X-ray pair distribution function (PDF) analysis to directly measure the solution-phase structure of intermediate clusters during the hydrolysis of bismuth di-salicylate (**S1**). This has been previously shown to form discrete bismuth oxide clusters capped by salicylate ions[11].

Measurements were performed in anhydrous (Sigma, ⩽ 0.03 % H_2O) DMF, (handled under Ar), and 'bench' conditions where DMF was handled in air. For the former, dynamic light scattering (DLS) detected only large aggregates (> 200 nm, Fig. 1a). However, after atmospheric exposure (24 hrs), 1.5 nm particles with a narrow size distribution were seen. Adding 10 % water by weight shifts the peak to 2.3 nm. This implies the presence of two magic size cluster species with tunable abundancies. Immediate growth of the small species was observed using bench DMF, even when sealed under Ar. The larger species again forms when more water is added. However, the size distributions were broader. The first step in the condensation hence occurs rapidly, and is perhaps catalysed with very small amounts

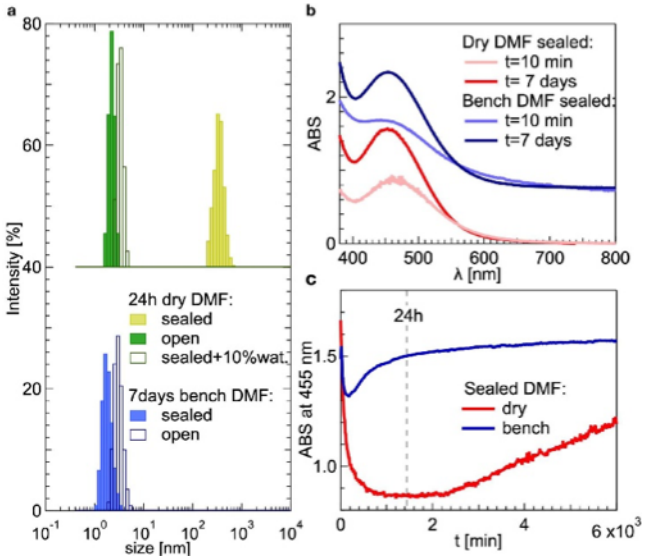

FIGURE 1. a, Samples in dry DMF (under Ar), show only large aggregates by DLS. Atmospheric exposure, or adding 10 % H_2O by volume yields $\{Bi_9O_7\}$ or $\{Bi_{38}O_{44}\}$ species. Solvent exposed to air (bottom) broadens the size distributions. **b,** Formation of the larger species in panel a causes an increase in intensity and sharpening of the UV-VIS peak at 450 nm. **c,** No change in the intensity at 450 nm is seen for sealed samples in dry DMF for > 30 hrs.

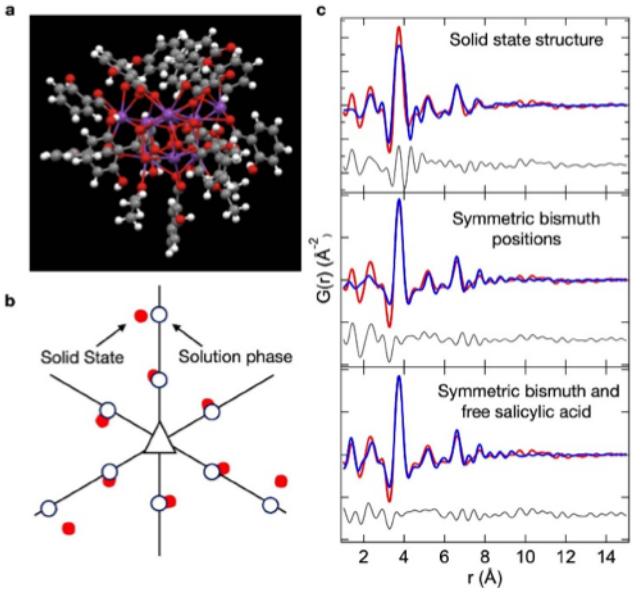

FIGURE 2. a, Solid-state model[10] for $[Bi_9O_7(HSal)_{13}]$, atoms are bismuth (purple), oxygen (red), carbon (grey) and hydrogen (white). **b,** The Bi positions have nearly three-fold point group symmetry. This symmetry was added for the solution phase fit. **c,** (top) The solid-state structure (blue) produces too broad Bi-Bi peaks (i.e. is too distorted), compared to the hydrolysis product (red) in cyclohexanone; (middle) The symmetric Bi positions produces the correct peak widths. (bottom) Adding free salicylic acid (~160 per cluster) fits the low-r features including the intense C-C distance at ~1.5 Å.

of water. Growth of the larger species is either slower, or only favourable over a certain water concentration.

All solutions were a vivid pink, showing broad peaks in UV-Vis spectra (Fig. 1b). For dry solvents/early times, this is asymmetric, with a long tail extending up to > 900 nm, implying very small, or a mixture of species[22]. At low bismuth concentration, a clear two-peak structure at 450 and 540 nm resolves, which is insensitive to water concentration (**S2**). This is also seen after 14 months of ageing mixtures of Bi_2O_3 and HSal in DMF (**S3**), and may reflect an intrinsic instability of Bi_2O_3 to solvolysis. As the [Bi] and [H_2O] increase, the 450 nm feature sharpens, and the signal above ca. 600 nm is quenched. Consistent with the DLS results, this indicates a well-defined, larger species (which is photoluminescent, **S4**). Time-dependent experiments performed at 450 nm confirm the link between solvent water content and kinetics. After an exponential decay caused by sedimentation, a rapid increase in intensity is found over 6-12 hrs for a sealed sample in bench DMF (Fig. 1c). In contrast, sealed samples in dry DMF show no reaction over periods of over 30 hrs.

To determine the structures of the species present, we used solution phase X-ray scattering. Briefly, data were measured with high energy X-rays (90-100 keV), an experimentally determined solvent background was subtracted, then Fourier transformation to real space was performed. This yields the PDF, which is a histogram of interatomic distances in the solute. We developed a modelling technique using point-group symmetry constraints and Debye function calculations (**SI**.) Our initial experiments (**S5**) were performed in five different solvents. The resulting PDFs fall in two groups, consistent with a small Bi-core (ca. 0.7 nm) and a large Bi-core (ca. 1.2 nm). Dry DMF produced the former, whereas bench DMF showed the larger cluster. We fingerprinted the species present, by calculating the PDFs of a wide range of Bi-oxo clusters from the CSD database (**S6**). The position and intensity of the peaks for the small species were matched by a reported[10] solid-state $[Bi_9O_7(HSal)_{13}]$ cluster (Fig. 2a). This structure is triclinic, with 27 fractional Bi coordinates. However, the calculated peak widths (Γ) were substantially larger than in the data (Fig. 2b). The calculated Γ contains three contributions, thermal displacements (σ^2), broadening from the finite momentum transfer (Qmax=14 Å^{-1}) and the dispersion of atomic distances in the model. Even when σ^2 was reduced to zero, we were unable to fit the peak widths, showing that the solid state model is measurably more distorted than the solvated cluster. Examining the $\{Bi_9O_7\}$ core, we noticed that the Bi positions make up a partially stellated octahedron, with nearly three-fold symmetry along one axis. Displacements away from these positions originate from lone pair distortions. We converted the model to cartesian coordinates, and imposed three-fold symmetry (Fig. 2c). This model retains the oxide positions and salicylate ligands, and the Bi positions can be refined with only two variables. This converged with a much better fit of the Bi-Bi peaks in the PDF, as the higher symmetry model reduces the peak widths (Fig. 2b). Complete ligand coverage fails to account for several sharp features at low-r, characteristic of organic bonding. We therefore added a contribution from free salicylate groups, consistent with a condensation reaction of smaller Bi species yielding free ligand and the $[Bi_9O_7(HSal)_{13}]$ cluster.

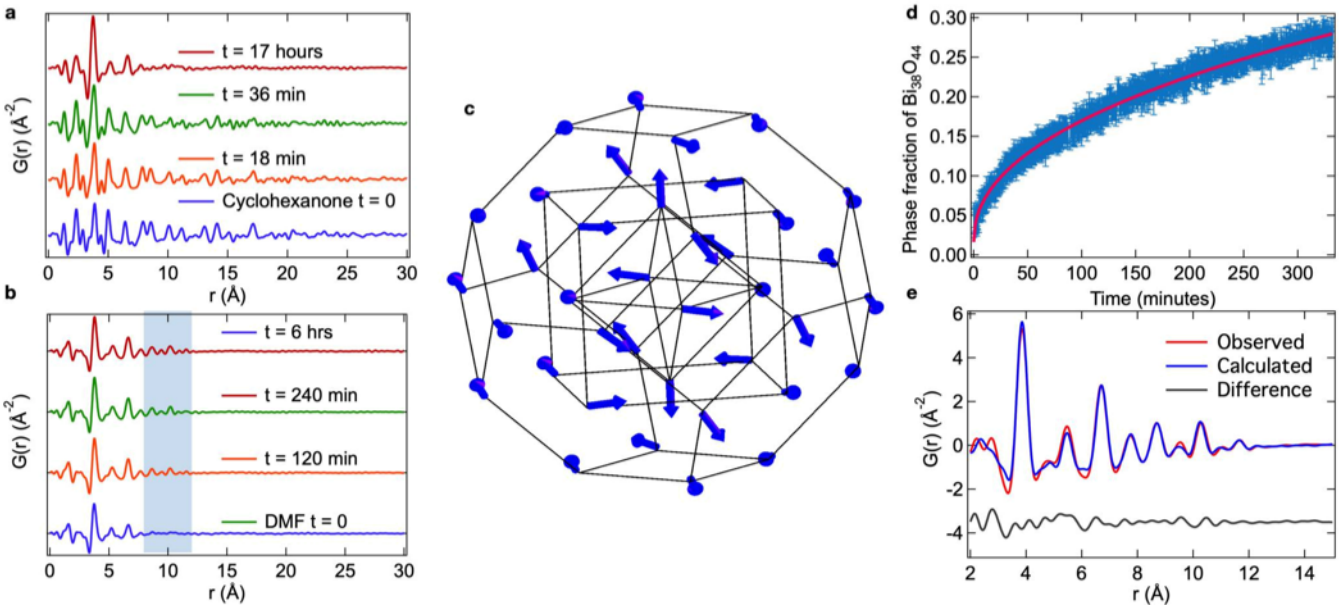

Figure 3. a, Time-resolved X-ray PDF data for a slurry of coordination polymer in cyclohexanone (open to the atmosphere). This reaction produces $[Bi_9O_7(HSal)_{13}]$ only. **b,** X-ray PDF data for a slurry of polymer in dry DMF (open to the atmosphere). This reaction rapidly produces $[Bi_9O_7(HSal)_{13}]$, which then converts to $[Bi_{38}O_{44}(Hsal)_{26}(H_2O)_4(DMF)_{18}]$. **c,** Parameterization of the lone-pair distortions of $\{Bi_{38}O_{44}\}$ in the solid state. The amplitude of this mode was refined against the experimental data. **d,** Time dependence of the $\{Bi_{38}O_{44}\}$ phase fractions in DMF. **e,** Final fit of the model described in the text to data from a sample produced in 10 % H_2O in DMF. This sample was sealed, and has aged for ~24 hours. A contribution from $\{Bi_9O_7\}$ is included at the ~30 % level.

Our time-resolved measurements (Fig.3a, b) directly show that the $\{Bi_9O_7\}$ cluster is the first product of hydrolysis. In a cyclohexanone slurry, sedimentation was slow enough to detect co-existence of polymer and $[Bi_9O_7(HSal)_{13}]$. No evidence of smaller species, e.g. monomers or dimers was seen. However, in dry DMF open to air, we detected the initial formation of $[Bi_9O_7(HSal)_{13}]$ before the slow (over 17 hrs) emergence of peaks at distances of up to 10 Å (Fig. 3b). This directly shows conversion into a larger species. Characteristic peaks in the PDF at 10 and 11.5 Å, were found to match the known[11] final hydrolysis product, $[Bi_{38}O_{44}(Hsal)_{26}$-$(H_2O)_4(DMF)_{18}]$.

Linear combination ruled out smaller species within our detection limit, giving the time evolution of the $\{Bi_{38}O_{44}\}$ phase fraction in Fig. 3d. The calculated peak widths were again too broad when using the reported[11] solid-state structure for $[Bi_{38}O_{44}(Hsal)_{26}(H_2O)_4(DMF)_{18}]$. This has a >30000 Å^3 unit cell with orthorhombic symmetry. The clusters have only two-fold symmetry, with 57 fractional coordinates for the Bi sites alone. We hence took inspiration from the observation that the $\{Bi_{38}O_{44}\}$ core is a distorted Keplerate[23], made up of shells of a nested octahedron, cube and truncated octahedron. Assuming that only the amplitude of the distortion is reduced in the solution phase, we parameterised it using the shifts shown in Fig. 3c.

This generates a model with a single parameter which describes the amplitude of the symmetry breaking Bi displacements[24]. While none of our samples showed purely the $\{Bi_{38}O_{44}\}$ clusters after ageing times of up to 24 hours, two phase fits of the above model with $[Bi_9O_7(HSal)_{13}]$, gave excellent fits with a small number (7) of parameters (Fig. 3e). The refined shifts of the Bi cations in the $\{Bi_{38}O_{44}\}$ species are much smaller than that found in the solid state model (ca. 0.15 vs 0.3 Å), which seems ubiquitous for this class of clusters.

To examine in more detail the structural changes upon solvating or crystallising the two clusters, we directly compared the distribution of Bi-Bi distances. For the solvated $\{Bi_9O_7\}$ and $\{Bi_{38}O_{44}\}$ cores, a much increased multiplicity is found for the distances in each coordination shell (Fig. 4a, 4b). However, there is little evidence for volume changes, since the average values remain similar. The main difference between the solution and solid state forms of these clusters appears to be a reduction in Bi^{3+} lone pair displacements. We note that other measurements, more sensitive to oxide displacements, may be needed to rule out alternative hypotheses related to disorder of this sub-lattice.

This result is not unexpected, since anisotropic packing interactions constrain molecular structures in the solid state[25]. It is however, extremely difficult to *prove* experimentally by any method other than solution phase X-ray scattering as developed here. We gained further insight into the electronic origins of distortions in $[Bi_9O_7(HSal)_{13}]$ by DFT structure relaxation, which used a continuum solvent model and simplified ligands (**S7**). This T = 0 K calculation retains the distorted Bi-O substructure, which is hence shown to be an intrinsic Jahn-Teller like electronic instability. We speculate that the observed higher-symmetry solvated structure is higher energy, and that electronic degeneracy is lifted upon crystallisation[26]. The importance of such inter-cluster interactions is supported by our vibrational spectroscopy measurement. In the simple octahedral species $[Bi_6OH_{12}]^{6+}$, the low-energy vibrational

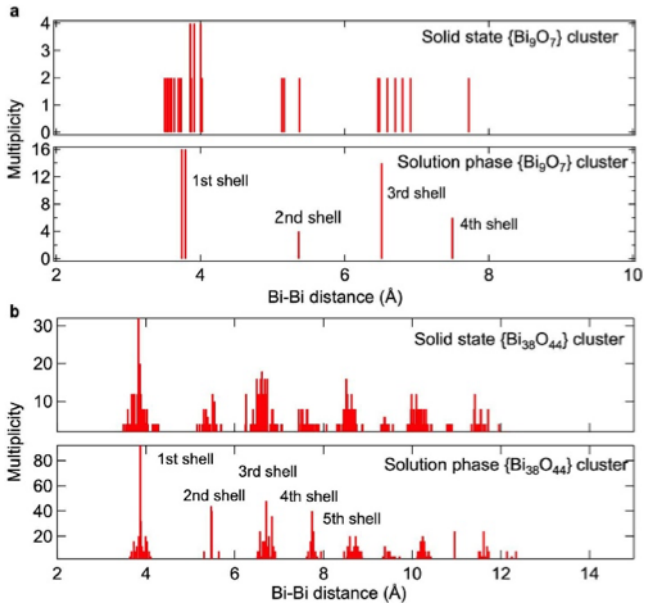

FIGURE 4. a, Bi-Bi distances determined from the $\{Bi_9O_7\}$ solid state structure model[10] with those from our refinements. The latter model not only fits our data better, but is higher symmetry. **b,** Comparison of the Bi-Bi distances determined from the $\{Bi_{38}O_{44}\}$ solid state structure model[10] with those from our refinements. The main structural change on solvation is a reduction in Bi^{3+} lone-pair displacements.

spectrum is almost unchanged on solvation[27]. However, for $[Bi_{38}O_{44}(Hsal)_{26}(H_2O)_4(DMF)_{18}]$, the metal-oxo modes are highly sensitive to the cluster environment. While clearly visible in single crystals, gentle grinding wipes out all but one Raman mode below 200 cm^{-1} (**S7**). In the solution phase, none are visible (**S8**). Together with the broad UV–Vis absorption bands, this shows that the solvated clusters undergo large and incoherent motions at room temperature[22,28].

In summary, detailed solution phase speciation detects new and previously unexplored complexity in the solvolysis of bismuth salicylate. The sensitivity of the reaction to small perturbations supports the hypothesis of a flat free-energy surface in unconventional nucleation and growth[13,14]. We directly probe the solute structure using X-ray scattering and symmetry constrained minimal models. This shows that, while magic-size clusters are trivially similar to frozen solid state analogues, they are significantly higher symmetry and higher energy. These clusters are hence structurally 'soft', explaining why they can be crystallised under appropriate conditions, while also remaining labile enough to grow into larger species. We speculate that the energetic barrier which renders such clusters metastable in solution, is comparable to the energy gain when the distorted solid state form is reached.

ASSOCIATED CONTENT

Supporting information is available free of charge, and consists of: Experimental section/methods Supporting figures S1 to S9 and details on the calculation of the pair distribution functions from models.

AUTHOR INFORMATION

Corresponding Authors

Tomislav Friščić - Department of Chemistry, McGill University, Montréal, QC H3A 0B8, Canada.
Email: tomislav.friscic@mcgill.ca
orcid.org/0000-0002-3921-7915

Simon A.J. Kimber - Laboratoire Interdisciplinaire Carnot de Bourgogne, UMR 6303 CNRS-Université Bourgogne Franche-Comté, 9 avenue Alain Savary, BP 47870, F-21078 Dijon Cedex, France.
Email: simon.kimber@u-bourgogne.fr
orcid.org/0000-0002-3969-5095

Authors

Daniel Szczerba - Laboratoire Interdisciplinaire Carnot de Bourgogne, UMR 6303 CNRS-Université Bourgogne Franche-Comté, 9 avenue Alain Savary, BP 47870, F-21078 Dijon Cedex, France

Davin Tan - Department of Chemistry, McGill University, Montréal, QC H3A 0B8, Canada

Jean-Louis Do - Department of Chemistry, McGill University, Montréal, QC H3A 0B8, Canada

Hatem M. Titi - Department of Chemistry, McGill University, Montréal, QC H3A 0B8, Canada

Siham Mouhtadi - Université Bourgogne Franche- Comté , Institut UTINAM-UMR, CNRS 6213, 16 Route de Gray, 25030 Besançon cedex, France

Denis Chaumont - Laboratoire Interdisciplinaire Carnot de Bourgogne, UMR 6303 CNRS-Université Bourgogne Franche-Comté, 9 avenue Alain Savary, BP 47870, F-21078 Dijon Cedex, France

María del Carmen Marco de Lucas – Laboratoire Interdisciplinaire Carnot de Bourgogne, UMR 6303 CNRS-Université Bourgogne Franche-Comté, 9 avenue Alain Savary, BP 47870, F-21078 Dijon Cedex, France

Nicolas Geoffroy - Laboratoire Interdisciplinaire Carnot de Bourgogne, UMR 6303 CNRS-Université Bourgogne Franche-Comté, 9 avenue Alain Savary, BP 47870, F-21078 Dijon Cedex, France

Michel Meyer - Insitut de Chimie Moléculaire de l'Université de Bourgogne, UMR 6302, CNRS, Université Bourgogne Franche Comté, 9 Avenue Alain Savary, BP 47870, 21078 Dijon cedex, France

Yoann Rousselin - Insitut de Chimie Moléculaire de l'Université de Bourgogne, UMR 6302, CNRS, Université Bourgogne Franche Comté, 9 Avenue Alain Savary, BP 47870, 21078 Dijon cedex, France

Jessica M. Hudspeth - European Synchrotron Radiation Facility, BP 156, 38042, Grenoble, France

Valérie Schwanen - University of Liège, Allée du six août, 11 - 4000 Liège, Belgium

Petra Spoerk-Erdely - Department Materials Science, Montanuniversität Leoben, Franz Josef-Strasse 18, 8700 Leoben, Austria.

Ann-Christin Dippel - Deutsches Elektronen- Synchrotron DESY, Notkestraße. 95, 22603 Hamburg, Germany

Oleh Ivashko - Deutsches Elektronen-Synchrotron DESY, Notkestraße. 95, 22603 Hamburg, Germany

Olof Gutowski - Deutsches Elektronen-Synchrotron DESY, Notkestraße. 95, 22603 Hamburg, Germany

Philipp Glaevecke - Deutsches Elektronen- Synchrotron DESY, Notkestraße. 95, 22603 Hamburg, Germany

Vasilli Bazhenov - European XFEL GmbH, Holzkoppel 4, 22869 Schenefeld, Germany

Ivan Halasz - Ruđer Boš ković Institute, Bijenička cesta 54, 10000 Zagreb, Croatia orcid.org/0000-0002-5248-4217

Mihails Arhangelskis - Faculty of Chemistry, University of Warsaw, 1 Pasteura St. 02-093 Warsaw, Poland

Notes

The authors declare no competing financial interests.

ACKNOWLEDGMENT

We acknowledge the European Synchrotron Radiation Facility for provision of synchrotron beam time on ID15B. We acknowledge DESY (Hamburg, Germany), a member of the Helmholtz Association HGF, for the provision of experimental facilities. Parts of this research were carried out at P21.1. We thank Sakura Pascarelli for her kind help in Hamburg, and the staff of ID15 at the ESRF for assistance with consumables. Agnieszka Poulain is acknowledged for support on the beam line. VS and PSE were funded by the ESRF-ILL International Summer Student Program. This work was supported by the EIPHI Graduate School (contract ANR-17-EURE-0002). Ce travail a été soutenu par le programme "Investissements d'Avenir", ISITE-BFC project (contract ANR- 15-IDEX-0003). We thank Agnés Birot for administrative support.

REFERENCES

1. Mjos, K. D. & Orvig, C. Metallodrugs in medicinal inorganic chemistry. Chemical reviews 114, 4540–4563 (2014).

2. Anthony, E. J. et al. Metallodrugs are unique: opportunities and challenges of discovery and development. Chemical Science 11, 12888–12917 (2020).

3. Sun, H., Li, H. & Sadler, P. J. The biological and medicinal chemistry of bismuth. Chemische Berichte 130, 669–681 (1997).

4. Lambert, J. & Midolo, P. The actions of bismuth in the treatment of Helicobacter pylori infection. Alimentary pharmacology & therapeutics 11, 27– 33 (1997).

5. Yuan, S. et al. Metallodrug ranitidine bismuth citrate suppresses SARS-CoV-2 replication and relieves virus-associated pneumonia in Syrian hamsters. Nature microbiology 5, 1439–1448 (2020).

6. Mehring, M., Mansfeld, D., Paalasmaa, S. & Schürmann, M. Polynuclear Bismuth-Oxo Clusters: Insight into the Formation Process of a Metal Oxide. Chemistry–A European Journal 12, 1767– 1781 (2006).

7. Mansfeld, D. et al. From $\{Bi_{22}O_{26}\}$ to Chiral Ligand-Protected $\{Bi_{38}O_{45}\}$-Based Bismuth Oxido Clusters. Chemistry-a European Journal 17, 14805 (2011).

8. Miersch, L. et al. Hydrolysis of a Basic Bismuth Nitrate—Formation and Stability of Novel Bismuth Oxido Clusters. Chemistry–A European Journal 17, 6985–6990 (2011).

9. Schlesinger, M., Miersch, L., Rüffer, T., Lang, H. & Mehring, M. Two Novel Nanoscaled Bismuth Oxido Clusters, $[Bi_{38}O_{45}(OMc)_{22}(C_8H_7SO_3)_2(DMSO)_6(H_2O)_{1.5}] \cdot 2.5\ H_2O$ and $[Bi_{38}O_{45}(HSal)_{22}(OMc)_2(DMSO)_{15}(H_2O)] \cdot DMSO \cdot 2\ H_2O$. Main Group Metal Chemistry 36, 11–19 (2013).

10. Andrews, P. C. et al. Towards a structural understanding of the anti-ulcer and anti-gastritis drug bismuth subsalicylate. Angewandte Chemie 118, 5766–5770 (2006).

11. André, V. et al. Mechanosynthesis of the metallodrug bismuth subsalicylate from Bi_2O_3 and structure of bismuth salicylate without auxiliary organic ligands. Angewandte Chemie 123, 8004– 8007 (2011).

12. Anker, A. S. et al. Structural Changes during the Growth of Atomically Precise Metal Oxido Nanoclusters from Combined Pair Distribution Function and Small-Angle X-ray Scattering Analysis. Angewandte Chemie 133, 2–12 (2021).

13. Gebauer, D., Kellermeier, M., Gale, J. D., Bergström, L. & Cölfen, H. Pre-nucleation clusters as solute precursors in crystallisation. Chemical Society Reviews 43, 2348–2371 (2014).

14. Lee, J., Yang, J., Kwon, S. G. & Hyeon, T. Nonclassical nucleation and growth of inorganic nanoparticles. Nature Reviews Materials 1, 1–16 (2016).

15. Gary, D. C., Terban, M. W., Billinge, S. J. & Cossairt, B. M. Two-step nucleation and growth of InP quantum dots via magic-sized cluster intermediates. Chemistry of Materials 27, 1432–1441 (2015).

16. Luan, C. et al. Four Types of CdTe Magic-Size Clusters from One Prenucleation Stage Sample at Room Temperature. The journal of physical chemistry letters 10, 4345–4353 (2019).

17. Jensen, K. M. et al. Polymorphism in magic-sized Au 144 (SR) 60 clusters. Nature communications 7, 1–8 (2016).

18. Williamson, C. B. et al. Chemically reversible isomerization of inorganic clusters. Science 363, 731–735 (2019).

19. Gebauer, D., Völkel, A. & Cölfen, H. Stable prenucleation calcium carbonate clusters. Science 322, 1819–1822 (2008).

20. Furrer, G., Phillips, B. L., Ulrich, K.-U., Pöthig, R. & Casey, W. H. The origin of aluminum flocs in polluted streams. Science 297, 2245–2247 (2002).

21. Soderholm, L., Almond, P. M., Skanthakumar, S., Wilson, R. E. & Burns, P. C. The structure of the plutonium oxide nanocluster [Pu38O56Cl54 (H2O) 8] 14-. Angewandte Chemie International Edition 47, 298–302 (2008).

22. Beecher, A. N. et al. Atomic structures and gram scale synthesis of three tetrahedral quantum dots. Journal of the American Chemical Society 136, 10645–10653 (2014).

23. Chandrasekhar, V., Metre, R. K. & Sahoo, D. Bi38 Oxocarboxylate Cages are Keplerates–Synthesis and Structural Characterization of Two Bi38 Oxocarboxylate Cages. European Journal of Inorganic Chemistry 2014, 164–171 (2014).

24. Perversi, G. et al. Co-emergence of magnetic order and structural fluctuations in magnetite. Nature communications 10, 1–6 (2019).

25. Steed, J. W. Should solid-state molecular packing have to obey the rules of crystallographic symmetry? CrystEngComm 5, 169–179 (2003).

26. Öpik, U. & Pryce, M. H. L. Studies of the Jahn- Teller effect. I. A survey of the static problem. Proceedings of the Royal Society of London. Series A. Mathematical and Physical Sciences 238, 425–447 (1957).

27. Maroni, V. A. & Spiro, T. G. The Vibrational Spectrum of the Hydrolytic Hexamer of Bismuth (III) 1a. Journal of the American Chemical Society 88, 1410–1412 (1966).

28. Voznyy, O., Mokkath, J. H., Jain, A., Sargent, E. H. & Schwingenschlögl, U. Computational study of magic-size CdSe clusters with complementary passivation by carboxylic and amine ligands. The Journal of Physical Chemistry C 120, 10015–10019 (2016).